A SINGLE CAMERA UNIT-BASED THREE-DIMENSIONAL SURFACE IMAGING TECHNIQUE

A Thesis

by

YINHE WANG

Submitted to the Graduate and Professional School of
Texas A&M University
in partial fulfillment of the requirements for the degree of

MASTER OF SCIENCE

Chair of Committee,	ChaBum Lee
Committee Members,	Bruce Tai
	Dinakar Sagapuram
Head of Department,	Guillermo Aguilar

May 2023

Major Subject: Mechanical Engineering

ABSTRACT

The main objective of this study is to develop a single-camera unit-based three-dimensional surface imaging technique that could be used to reduce the disparity error in three-dimensional (3D) image reconstruction and simplify the calibration process of the imaging system. The current advanced stereoscopic 3D imaging system uses a pair of imaging devices (e.g., complementary metal-oxide semiconductor (CMOS) or charge-coupled device (CCD)), imaging lenses, and other accessories (e.g., light sources, polarizing filters) and diffusers.) To reconstruct the 3D scene, the system needs to calibrate the camera and compute a disparity map. However, in most cases in the industry, a pair of imaging devices is not ideally identical, so it is a necessary step to finely adjust and compensate for camera orientation, lens focal length, and intrinsic parameters for each camera. More importantly, conventional stereoscopic systems may respond differently to incident light reflected from the target surface. It is possible for the pixel information in the left and right images to be slightly different. This results in an increase in disparity error, even though the stereovision system is calibrated and compensated for rotation and vertical offsets between two cameras. This thesis aims to solve the aforementioned challenges by proposing a new stereo vision scheme based on only one camera to obtain target 3D data by 3D image reconstruction of two images obtained from two different camera positions.

DEDICATION

This thesis is dedicated to my family, who always supports me and prays for my success.

And most of all,

to the Almighty God, my source of wisdom, strength, and courage.

Without whom none of my works would be possible.

ACKNOWLEDGEMENTS

To all the people who helped and supported me in completing this thesis, I would like to express my sincere gratitude.

First and foremost, I would like to thank my major research advisor in the J. Mike Walker 66' Department of Mechanical Engineering, Dr. ChaBum Lee, for his continuous guidance and support throughout my graduate career. His constant inspiration, tireless enthusiasm, experience, patience, and valuable advice have led me to the successful completion of this thesis.

I would also like to thank my committee members, Dr. Bruce Tai and Dr. Dinakar Sagapuram, for allowing me valuable time to defend my thesis and for their comments and suggestions regarding my research.

I would also like to thank all the members of the Precision Metrology and Inspection Group (PMIG) for their cooperation, suggestions, and willingness to help my research and make it a great experience towards my academic goal at Texas A&M University.

I would also like to thank Honeywell Federal Manufacturing & Technologies LLC for the project (DE-NA0002839) and the National Science Foundation for the project (CMMI #2124999).

Finally, thank you to my beloved family and friends for encouraging me, praying for me, loving me, and allowing me to step forward when I am afraid.

CONTRIBUTORS AND FUNDING SOURCES

Contributors

This work was supervised by a thesis committee consisting of Professor Dr. ChaBum Lee of the J. Mike Walker 66' Department of Mechanical Engineering and Professor Dr. Bruce Tai of the J. Mike Walker 66' Department of Mechanical Engineering and Professor Dr. Dinakar Sagapuram of the Department of Engineering Technology & Industrial Distribution.

Acknowledgements related to each chapter are detailed in the subsection of each chapter, and the thesis was completed independently by the student.

Funding Source

The graduate study was supported by the J. Mike Walker 66' Mechanical Engineering Department at Texas A&M University.

NOMENCLATURE

3D	Three Dimensional
CMOS	Complementary Metal Oxide Semiconductor
CCD	Charge Coupled Device
PMIG	Precision Metrology and Inspection Group
AI	Artificial Intelligence
CMM	Coordinate Measuring Machine
SEM	Scanning Electron Microscope
AFM	Atomic Force Microscope
TOF	Time-of-Flight
LiDAR	Light Detection and Ranging
BSV	Binocular Stereo Vision
MVS	Multiple View Stereo
VR	Virtual Reality
LDW	Lane Departure Warning
SLAM	Simultaneous Localization and Mapping
SFM	Structure from Motion
SURF	Speeded Up Robust Features
RANSAC	Random Sample Consensus
SRS	Spatial Reference System
RP	Pose Repeatability
AP	Pose Accuracy

NAN	Not a Number
SSR	Regression Aum of Squares
SST	Total Sum of Squares

TABLE OF CONTENTS

Page

LIST OF FIGURES

Page

LIST OF TABLES

Page

1. INTRODUCTION

3D surface imaging as a non-contact surface measurement method is becoming popular in a variety of market segments such as industrial metrology, manufacturing, medical diagnosis, scientific research, and so on [1-4]. Benefiting from its non-contact characteristics, the 3D surface imaging technique has the characteristics of fast response and easy operation [5,6]. As the technology improves by leaps and bounds, researchers have adapted to numerous applications in many ways, combining various 3D surface imaging schemes, positioning and coordinate measurement, and powerful software technology including artificial intelligence (AI) [7]. Over the past half century, numerous 3D surface imaging techniques have been introduced: stereoscopy [8,9], strobe stereoscopy [10-12], structured light 3D scanning [13-15], time-of-flight scanning [16], interferometry [17], holographic imaging [18], and so on.

Stereoscopy is one of the 3D surface imaging techniques mentioned above. It is widely used in the industry due to its low cost and compact configuration. The stereoscopy technique is implemented using a pair of imaging devices to acquire multi-view images of the target at different locations. Use the principle of triangulation to determine the 3D position and coordinates of the target. Conventional stereoscopy that utilizes a pair of imaging devices (e.g., CCD or CMOS), Imaging lenses and other accessories such as polarizers, diffusers, light sources, etc. requires camera calibration and computation of a disparity map. Here, a pair of the above-mentioned devices are not ideally identical, so the camera parameters, lens focal length, and camera alignment must be fine-tuned and compensated. Also, two camera-based systems might react differently to the incident light reflected from the target surface, so the pixel information in the left and right images might be slightly different. This results in an increase in disparity error although the

stereovision system is calibrated and compensated for the rotation and vertical offsets between two cameras.

The proposed three-dimensional imaging technology based on a single camera unit has the following capabilities: 1) Complete 3D positioning and coordinate measurement with only one imaging device and motion control platform or robotic arm, which means lower investment and maintenance costs, 2) Simple and convenient calibration process of the imaging system, 3) Adjustable baseline distance and tilt angle for more complex application environments and error compensation, 4) By specially designed backgrounds to reduce disparity error when for objects lacking surface features, 5) Finally, extraction of surface features and accurate thickness information of more detailed targets through image processing. As a result, the single camera unit-based three-dimensional surface imaging technique design in the PMIG can achieve a mean disparity error ≤ 0.26 in the camera pixel error when doing 3D reconstruction and thickness measurement.

1.1. Thesis Outline

This thesis is divided into five chapters. Each chapter has an overview showing the main topic discussed in that chapter. The technology background for the following chapter is explained in the detailed preface.

The second chapter provides an overview of 3D reconstruction measurement methods, including an explanation of the technology used in this work, the application scenario, the characteristics of each technology, and the development map of 3D surface imaging technology.

The third chapter presents the design of the experimental setup and the methods used for image processing and feature extraction. The results are also compared and discussed in terms of calibration accuracy and 3D reconstruction accuracy.

The fourth chapter focuses on the measurement error analysis of the single camera unit based three-dimensional surface imaging technique.

Finally, the fifth chapter will briefly summarize and discuss the main results and discuss future work.

1.2. References

[1] Shaukat, Affan, et al. "Towards camera-LIDAR fusion-based terrain modelling for planetary surfaces: Review and analysis." Sensors 16.11 (2016): 1952.

[2] Logozzo, Silvia, et al. "Recent advances in dental optics–Part I: 3D intraoral scanners for restorative dentistry." Optics and Lasers in Engineering 54 (2014): 203-221.

[3] Zhang, Zhengyou. "Microsoft kinect sensor and its effect." IEEE multimedia 19.2 (2012): 4-10.

[4] Yang, Sung-Pyo, et al. "Compact stereo endoscopic camera using microprism arrays." Optics letters 41.6 (2016): 1285-1288.

[5] Geng, Jason. "Structured-light 3D surface imaging: a tutorial." Advances in Optics and Photonics 3.2 (2011): 128-160.

[6] Yang, Sung-Pyo, et al. "Optical MEMS devices for compact 3D surface imaging cameras." Micro and Nano Systems Letters 7 (2019): 1-9.

[7] Hamid, Mohd Saad, et al. "Stereo matching algorithm based on deep learning: A survey." Journal of King Saud University-Computer and Information Sciences 34.5 (2022): 1663-1673.

[8] Chen, Fanxiu, et al. "Full-field 3D measurement using multi-camera digital image correlation system." Optics and Lasers in Engineering 51.9 (2013): 1044-1052.

[9] Zhang, Yiwei, et al. "A fast 3D reconstruction system with a low-cost camera accessory." Scientific reports 5.1 (2015): 10909.

[10] Zhang, Song. "Recent progresses on real-time 3D shape measurement using digital fringe projection techniques." Optics and lasers in engineering 48.2 (2010): 149-158.

[11] Lee, ChaBum, and Xiangyu Guo. "Spatially resolved stereoscopic surface profiling by using a feature-selective segmentation and merging technique." Surface Topography: Metrology and Properties 10.1 (2022): 014002.

[12] Guo, Xiangyu, and ChaBum Lee. "Fluorescence strobo-stereoscopy for specular reflection-suppressed full field of view imaging." Measurement 192 (2022): 110907.

[13] Guo, Xiangyu, and ChaBum Lee. "Preliminary study of phase-shifting strobo-stereoscopy for cutting tool monitoring." Journal of Manufacturing Processes 64 (2021): 1214-1222.

[14] Clancy, Neil T., et al. "Spectrally encoded fiber-based structured lighting probe for intraoperative 3D imaging." Biomedical Optics Express 2.11 (2011): 3119-3128.

[15] Schmalz, Christoph, et al. "An endoscopic 3D scanner based on structured light." Medical image analysis 16.5 (2012): 1063-1072.

[16] Velten, Andreas, et al. "Recovering three-dimensional shape around a corner using ultrafast time-of-flight imaging." Nature communications 3.1 (2012): 745.

[17] Chen, Liang-Chia, et al. "3-D surface profilometry using simultaneous phase-shifting interferometry." Optics Communications 283.18 (2010): 3376-3382.

[18] Su, Ting-Wei, et al. "Multi-angle lensless digital holography for depth resolved imaging on a chip." Optics express 18.9 (2010): 9690-9711.

2. A REVIEW: CURRENT METHODOLOGY OF 3D SURFACE RECONSTRUCTION AND ANALYSIS

2.1. Overview

With the development of image quality and computability, and the urgent need for fast and accurate inspection, the importance of non-contact inspection techniques has been recognized by industry and academia. Compared to traditional probe scanning such as coordinate measuring machines (CMMs), non-contact inspection has significant advantages in detection speed, operation, and maintenance costs. Although there are currently some non-contact inspection solutions provided by equipment suppliers, these methods are time-consuming, and most of them require additional steps to achieve geometry measurement process, such as scanning electron microscope (SEM), atomic force microscope (AFM), which are not the preferred choice for industry, especially assembly line production environments [1]. In this review, the current and previous methods of 3D reconstruction are presented and the current challenges are summarized. The technologies in the novel solution proposed in the thesis and its potential are also presented.

2.2. Preface

2.2.1. 3D Shape Acquisition

3D shape acquisition can be divided into contact and non-contact techniques [2]. Compared with non-contact techniques, contact techniques are more mature and have been used in the industry earlier. The advantage of contact measurement is high measurement accuracy, which is suitable for the precision of the three structural parameters of small workpieces, and its precision can reach the nanometer level [3,4]. But contact measurement is severely limited by the shape of the measuring tool and the target to be measured, the cause is limited to use for the large

measurement area. And the calibration of contact measurement techniques is complicated and time-consuming, for CMM measuring instruments of the displacement probe many errors caused by the radius of the displacement probe must be properly compensated to ensure the accuracy of measurement. And cosine errors can occur if the detector and measurement target surfaces are not aligned, as shown in Figure 2.1 [5]. The fatal flaw of contact measurement techniques is that they run the risk of damaging the sample under test. Even with CMMs, there is still a risk of the probe scratching the surface of the target, especially when measuring non-rigid bodies [6-9].

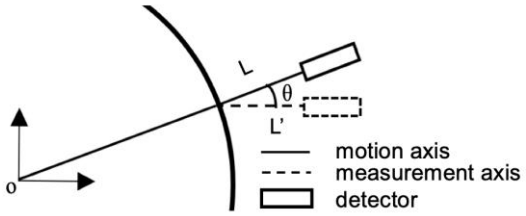

Figure 2.1. Schematic of the cosine error [5].

$$L' = L \cdot cos\theta \tag{2.1}$$

$$\varepsilon_c = L - L' = L(1 - cos\theta) \tag{2.2}$$

where L is the actual displacement, L' is the measured displacement, θ is the misalignment angle, and ε_c is the cosine error.

To overcome the above limitations of contact measurement, the non-contact surface measurement method is becoming popular in a variety of markets, and the technology can be adapted in many ways for numerous applications [10,11]. The advantage of non-contact techniques is the speed of measurement, which typically measures areas rather than single points on a target [12-16]. The non-contact techniques commonly used in the industry are basically based on the

principle of reflection. Optical-based techniques occupy a large share of the non-contact market due to their high accuracy and low cost. Beyond visible or infrared wavelengths, acoustic detection and ranging are the most popular non-contact options. An overview of the above techniques is summarized in Figure. 2.2.

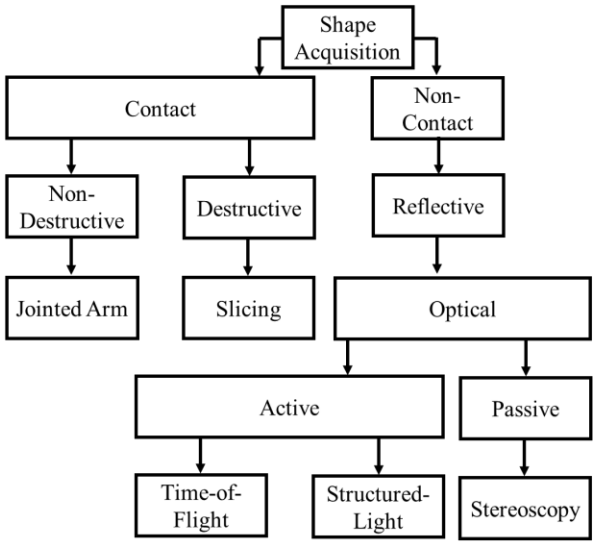

Figure 2.2. Summary of 3D shape acquisition techniques.

2.2.2. Active measurement

Active measurement requires the instrument to actively transmit controllable signals (sound waves, electromagnetic waves, visible light, lasers, etc.) to the target being measured. The surface characteristics of the target are calculated by comparing the transmitted signal and the feedback signal. A 3D reconstruction of the entire target can be obtained by scanning.

2.2.2.1. Time of Flight

Time of Flight (TOF) is a mature 3D shape measurement technique whose earliest application can be traced back to ultrasonic distance measurement a century ago. The principle of TOF is to load a light-emitting element, and the photos emitted by the light-emitting element are

reflected after hitting the surface of the object. By using a receiver, the photos emitted and reflected by the light-emitting element can be detected to calculate the time-of-flight of the photon. The distance of the photon flight can be obtained from the photon flight time. Figure 2.3 illustrates the working principle of a single-pixel TOF system.

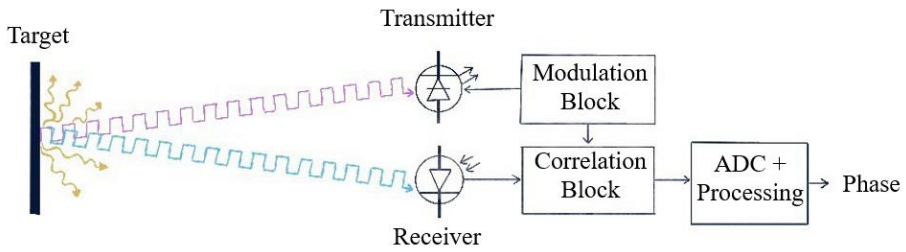

Figure 2.3. Time-of-flight transmission, reflection, and reception principle.

Due to its simple operating principle, it has a very wide range of industrial applications [17]. 3D cameras from Sony Depthsensing Solutions mainly use this technology. This technology has been widely used for military scanning [18] or Light Detection and Ranging (LiDAR) in autonomous vehicles [19]. However, this method offers lower resolution compared to stroboscopy and structured light scanning methods, is sensitive to lighting conditions, and is difficult to calibrate the system.

2.2.2.2. Structured-Light

The basic principle of structured light based camera technology is to introduce a laser projector and place a special stripe pattern outside it, when the laser beam is projected and imaged through the stripe pattern, it will be refracted so that the final landing point of the laser light on the surface of the object will be shifted. This allows us to use a camera to detect and collect the pattern projected on the surface of the object, and calculate the position and thickness information of the

object through the pattern displacement change algorithm, and then restore the entire 3D space, which is essentially a triangulation-based technique [20].

A classic structured light system is laser triangulation [21], shown in Figure 2.4. The system obtains the position and coordinates of the target by localizing the laser spot projected by the laser pointer using equations 2.3 and 2.4. This method is highly dependent on the performance of the camera and stripe pattern generator, and relies on the displacement of the landing point after laser refraction, so its measurement range is limited. Since the displacement caused by refraction is not obvious, measuring out of range can lead to errors in the calculated thickness information.

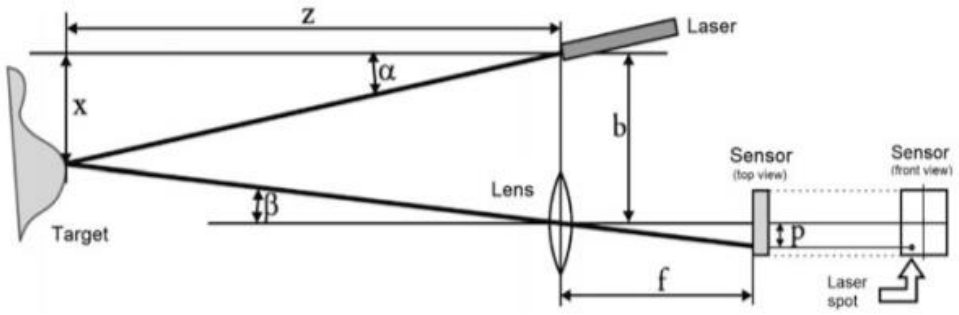

Figure 2.4. Triangulation with a single laser spot [21].

$$z = \frac{b}{\tan(\alpha) + \tan(\beta)} \tag{2.3}$$

$$x = z * \tan(\alpha) \tag{2.4}$$

2.2.3. Passive measurement

Passive measurements use optical and geometric relationships to measure the thickness of a target and its three-dimensional features [22]. Compared to active measurements, their

equipment and principle are simpler and more stable. These advantages make it occupy a larger market share in non-contact measurement.

2.2.3.1. Multi-camera

This technique requires at least two or more imaging devices to simultaneously acquire image information of the target [23-26]. It is a bionic design inspired by the compound eye of insects or the eyes of humans [27,28]. It works by comparing the disparity between different image positions and then converting it into thickness information to complete the 3D reconstruction of the target.

2.2.3.2. Stereoscopic

The stereoscopic system is one of the most common applications of multi-camera technology [29,30]. Stereoscopic calculates thickness information based on geometric principles. Since the intrinsic and extrinsic parameters of the two imaging devices are known. By finding the target position in different images, the thickness of the object from the camera through the algorithm [31-33]. Stereoscopic system relies entirely on computer vision algorithms to achieve 3D reconstruction, and its technical cost and power consumption requirements are much lower than structured light or TOF.

The working principle of the single-camera unit-based three-dimensional surface imaging technique introduced in this theory is based on stereoscopy. The details and application will be introduced in 2.3.3.

2.3. 3D motion stereo vision measurement

Based on the number of imaging devices, stereo vision motion measurement can be divided into binocular stereo vision (BSV), multiple view stereo (MVS), and single camera stereo vision [34].

2.3.1. 3D reconstruction based on BSV

In binocular stereo vision, two imaging devices are required to capture images of the target at different locations or orientations at the same time [35-37]. It is a bionic design inspired by the 3D perception of the human eye. Its working principle is to compare the disparity between different image positions and then convert it into depth information to complete the 3D reconstruction. Taking advantage of the computer's data processing capabilities, the machine vision algorithm is able to perceive and process images faster and more accurately than the human eye in most cases, which is conducive to image post-processing such as feature point extraction and so on. Based on these advantages, the development of binocular stereo vision technology has attracted the attention of academia and industry [38-39]. It is suitable for a wide range of applications due to its non-contact measurement and optical-based characteristics.

Wang et al. recently introduced a golf ball tracking system that uses a high-speed stereo camera for in-process measurement of golf feature extraction, trajectory analysis, speed detection, etc. It can track the golf ball motion at a speed of up to 360 km/h under normal indoor lighting conditions, and the experimental setup is shown in Figure 2.5 [40].

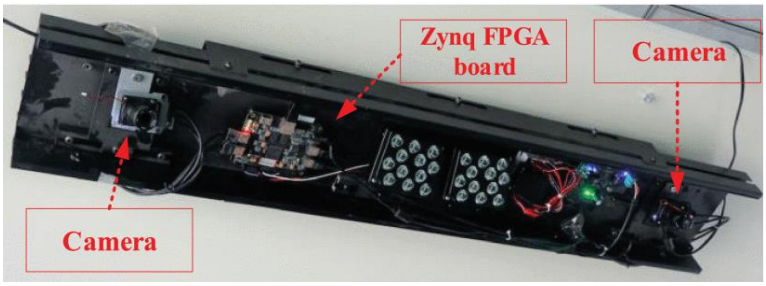

Figure 2.5. High-speed stereo vision system for golf ball tracking [40].

As shown in Figure 2.6, Guo et al. recently introduced strobe stereoscopy, which combines stereoscopy and stroboscopy for in-process measurement of cutting tool geometry and reconstruction of 360-degree full-view 3D images to monitor tool conditions [41-43].

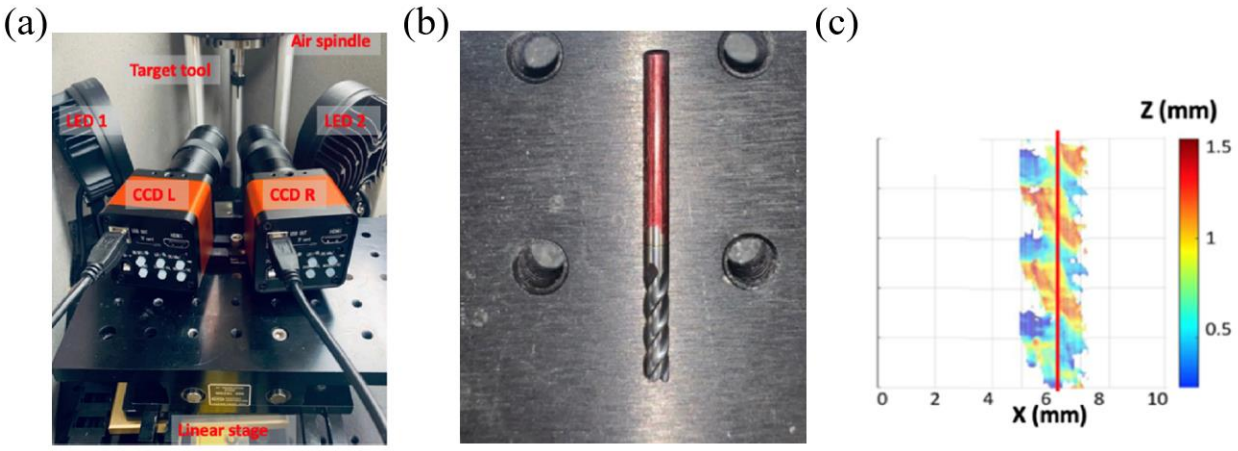

Figure 2.6. (a) Experimental setup of the proposed method, (b) Experimental target end mill sample, (c) Phase-locked surface map of the end mill [43].

As shown in Figure 2.7, Japanese researchers use two cameras to capture the features of human facial layout and realize the real-time measurement of human head pose and gaze direction through the features in the image [44].

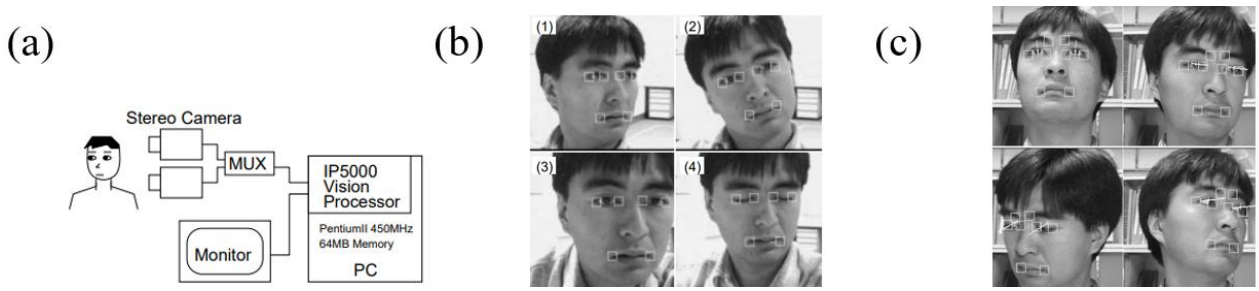

Figure 2.7. a) Experimental setup of the proposed method, b) Results of face tracking in different situations, c) Results of gaze direction detection [44].

With the progress of today's era and the development of science and technology, stereo vision motion measurement technology has developed rapidly. Binocular stereo vision does not require any additional equipment for measurement, and it can completely rely on optical and geometric recombination detection of target object features. Due to its excellent measurement performance, it is becoming popular in a variety of market segments, such as virtual reality (VR), measurement and inspection, manufacturing, medical diagnosis, video game entertainment, and so on [45-49]. Currently, common applications include lane departure warning (LDW), 3D scanning, etc., as shown in Figure 2.8.

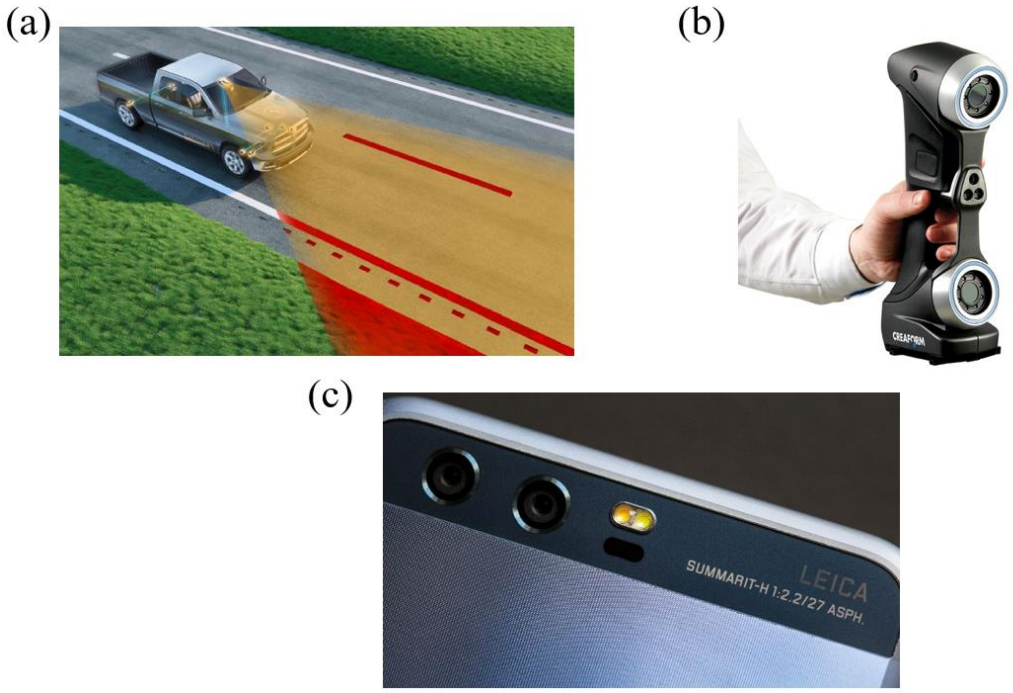

Figure 2.8. Common stereo vision motion measurement applications: (a) lane departure warning, (b) handheld 3D scanner, (c) smartphone binocular camera.

2.3.2. 3D reconstruction based on MVS

MVS technology is a general term for a group of technologies that use stereo matching and more than two image acquisition devices. MVS is often confused with Simultaneous Localization and Mapping (SLAM) and Structure from Motion (SFM), but there is a fundamental difference between them. MVS estimates 3D structure from known camera positions, while SLAM and SFM recover 3D structure from unknown camera positions [50].

The 3D reconstruction based on MVS can be roughly divided into three steps. First, multiple imaging devices are used to collect images of the measured sample, and then the camera parameters of each imaging device are calculated. Finally, a set of images and corresponding camera parameters are used to reconstruct the 3D geometry of the measured sample [51-53], as shown in Figure 2.9.

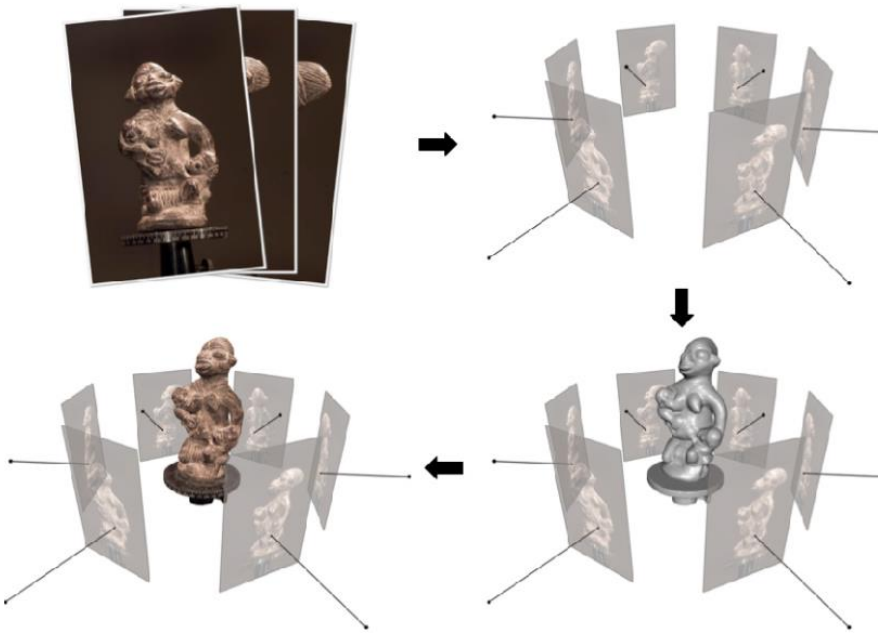

Figure 2.9. Example of a multi-view stereo pipeline. Clockwise: input images, posed images, reconstructed 3D geometry, textured 3D geometry [54].

Since MVS has excellent 3D reconstruction performance, many companies are engaged in research and development of related products, including Qualisys, Natural Point, etc. The German company CONTEMPLAS GmbH develops innovative solutions for professional motion analysis for athletes and fitness enthusiasts. TEMPLO is a popular motion capture system developed by the company [55]. As shown in Figure 2.10, their system captures motion from all perspectives with synchronized multi-camera systems from different perspectives, and the data has been further processed and analyzed to provide athletes with proper training analysis and planning, such as posture and strength.

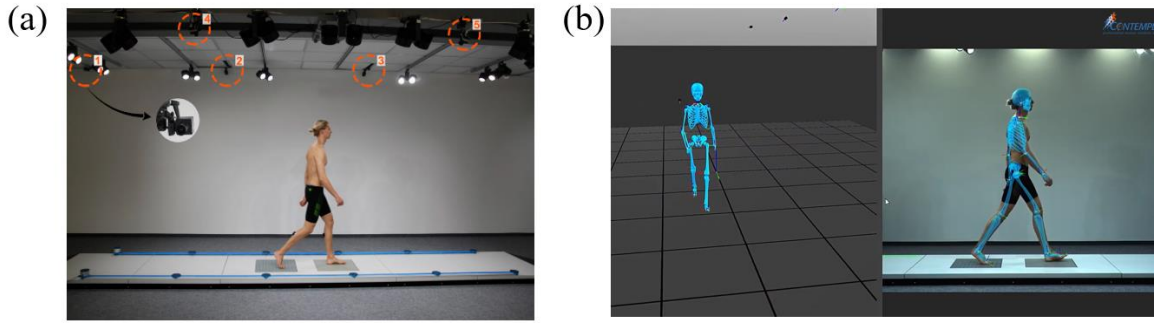

Figure 2.10. TEMPLO Motion Capture System: (a) Multi-camera system with 5 cameras, (b) 3D markerless tracking.

2.3.3. 3D reconstruction based on single camera stereo vision

Single camera stereoscopy requires only one imaging device to obtain the three-dimensional information of the measured object [56,57]. The principle is based on BSV: by moving the target or the imaging devices, two images of the target at different locations are obtained by scanning. The 3D surface image can then be reconstructed using the stereoscopy algorithm [58]. Compared to BSV, single-camera-based stereoscopy has attracted widespread attention due to its simple structure, easy implementation, and convenient on-site calibration [59-61].

A thickness measurement technique based on stereo vision with integrated camera rotation was recently presented by Lin et al. The scheme is shown in Figure 2.11. The camera was mounted on a shaft motion motor, and it was moved by the motor to obtain two images of the different positions of the target. However, the images obtained at this time cannot be directly reconstructed in 3D because the two images have inconsistent orientations. In this case, the camera's rotation matrix must be calibrated so that the two images can be properly aligned. Robust Features (SURF) and Random Sample Consensus (RANSAC) algorithms were then used to facilitate feature

extraction and correspondence matching. The results show that the three-dimensional thickness of simply shaped objects can be calculated [62].

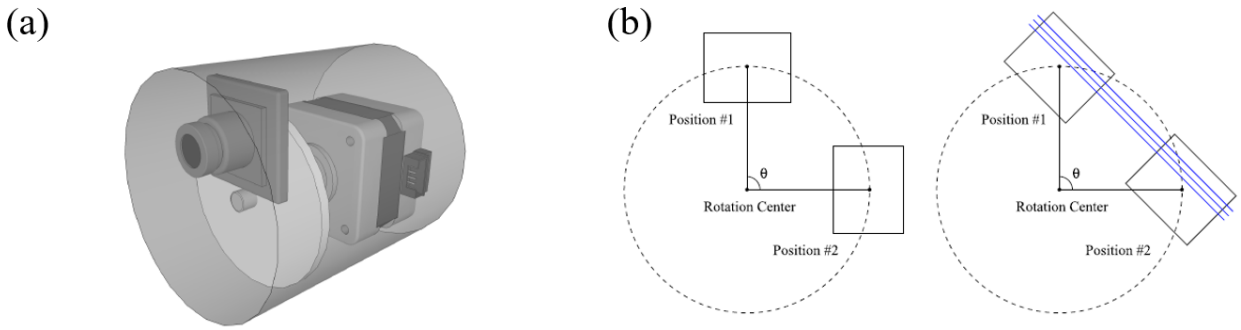

Figure 2.11. (a) Schematic of the stereo from sensor rotation design, (b) rectification of a stereo image pair based on the sensor rotation angle [62].

As shown in Figure. 2.12, Zhu et al. presented the design and calibration of a single-camera-based stereo vision sensor. This system uses one image capture device and two optical reflectors. If the optical path is properly designed, the reflectors can divide the effective field of view of the camera image into two symmetrical regions. Each symmetrical region can be equivalent to one camera system, making the entire imaging system equivalent to a BSV system [63].

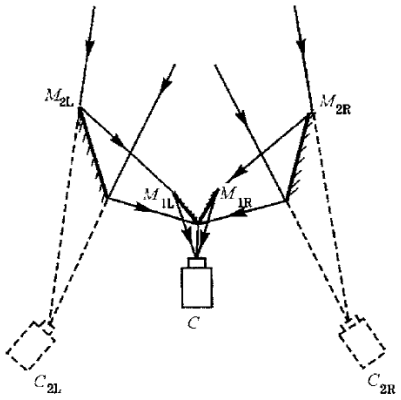

Where $M_{1L}, M_{1R}, M_{2L}, M_{2R}$ are two couples of symmetrical reflectors. C is the real camera and C_{2L}, C_{2R} are two virtual cameras.

Figure 2.12. The optical path of the single camera stereo vision sensor [63].

In conclusion, single camera stereoscopy cannot directly infer the 3D reconstruction of the measured target. This is because the obtained image features contain only 2D information. Additional information is needed to obtain the 3D information of the target [64,65]. It is well known that 2D and 3D information are not directly related. We can understand the relationship between them as non-linear. A scaling factor β is needed to restore the relationship between them. Additional equipment such as the axis motion motor and optical reflectors mentioned above are required to obtain the scaling factor [63]. This will increase its manufacturing cost and equipment complexity. But in most cases, even with the additional equipment, the cost is still lower than that of the traditional BSV system. This equipment often provides the advantage of a single camera stereo system, such as simplifying the calibration process and improving the measurement accuracy. At present, there are very few scientific research projects and related products based on single camera stereoscopy, which leaves a lot of development opportunities.

2.4. Summary

The review highlights the importance of the quality of 3D reconstruction and the reasons for the increasing need for optics-based non-contact 3D measurement, especially single-camera based. However, most of the research is still at the theoretical stage with very limited ability to perform 3D reconstructions. And there are very few commercially available devices that can perform 3D measurements with a single imaging device. Most of the available methods are based on reflectance. These technologies required professional optical path calibration, which is not industry friendly, especially in a production environment. And the single camera system based on reflectors is very sensitive to light such as reflections, illumination, or shadows. As a result, its measurement stability and application scenarios are lower than those of traditional optics-based non-contact 3D measurement, which greatly reduces its practicality. A novel single camera stereoscopy is needed to overcome the above shortcomings and fill the current market gap.

2.5. References

[1] Guo, Xiangyu, and ChaBum Lee. "Preliminary study of phase-shifting strobo-stereoscopy for cutting tool monitoring." Journal of Manufacturing Processes 64 (2021): 1214-1222.

[2] Shan, Dongri, Yingling Ke, and Yunfeng Liu. "Study on measurement planning of complex surface in reverse engineering." Zhongguo Jixie Gongcheng/China Mechanical Engineering 14.1 (2003): 9-12.

[3] Huang, Qiang-Xian, et al. "Nano-CMM stage with zero Abbe error and its error analysis." Guangxue Jingmi Gongcheng(Optics and Precision Engineering) 21.3 (2013): 664-671.

[4] Takamasu, Kiyoshi, et al. "Development of nano-CMM and parallel-CMM–CMM in the 21th century." International Dimensional Metrology Workshop. 1999.

[5] Guo, Xiangyu, and ChaBum Lee. "Cosine Error-Free Metrology Tool Path Planning for Thickness Profile Measurements." Journal of Manufacturing Science and Engineering 143.4 (2021).

[6] Herbsleb, James D., and Dennis R. Goldenson. "A systematic survey of CMM experience and results." Proceedings of IEEE 18th International Conference on Software Engineering. IEEE, 1996.

[7] Balsamo, Alessandro, et al. "Evaluation of CMM uncertainty through Monte Carlo simulations." CIRP Annals 48.1 (1999): 425-428.

[8] Estler, W. Tyler, et al. "Error compensation for CMM touch trigger probes." Precision Engineering 19.2-3 (1996): 85-97.

[9] Barakat, N. A., M. A. Elbestawi, and A. D. Spence. "Kinematic and geometric error compensation of a coordinate measuring machine." International Journal of Machine Tools and Manufacture 40.6 (2000): 833-850.

[10] Li, J. L., Q. Q. Xin, and L. Tian. "A review of online measurement method for large forgings." The Journal of New Industrialization 24.1 (2014): 59-64.

[11] Kumar, B. M., and M. M. Ratnam. "Machine vision method for non-contact measurement of surface roughness of a rotating workpiece." Sensor review 35.1 (2015): 10-19.

[12] Xu, XiaoMei, and Hong Hu. "Development of non-contact surface roughness measurement in last decades." 2009 International Conference on Measuring Technology and Mechatronics Automation. Vol. 1. IEEE, 2009.

[13] DeFisher, Scott, Michael Bechtold, and David Mohring. "A non-contact surface measurement system for freeform and conformal optics." Window and Dome Technologies and Materials XII. Vol. 8016. SPIE, 2011..

[14] Jolic, K. I., C. R. Nagarajah, and W. Thompson. "Non-contact, optically based measurement of surface roughness of ceramics." Measurement science and technology 5.6 (1994): 671.

[15] Fan, K. C. "A non-contact automatic measurement for free-form surface profiles." Computer integrated Manufacturing systems 10.4 (1997): 277-285. Ziwei, Liu, et al. "Theory and implementation of depth photography." Infrared and Laser Engineering 45.7 (2016): 726001-0726001.

[16] Edmondson, Vikki, et al. "Improved non-contact 3D field and processing techniques to achieve macrotexture characterisation of pavements." Construction and Building Materials 227 (2019): 116693.

[17] Li, Larry. "Time-of-flight camera—An introduction." Technical white paper SLOA190B (2014).

[18] Marino, Richard M., and William R. Davis. "Jigsaw: a foliage-penetrating 3D imaging laser radar system." Lincoln Laboratory Journal 15.1 (2005): 23-36.

[19] Yoo, Han Woong, et al. "MEMS-based lidar for autonomous driving." e & i Elektrotechnik und Informationstechnik (2018).

[20] Xiaojia, Wang, Gao Jun, and Wang Lei. "Survey on the laser triangulation." Chinese Journal of Scientific Instrument 25.4 (2004): 601-604.

[21] Giancola, Silvio, Matteo Valenti, and Remo Sala. A survey on 3D cameras: Metrological comparison of time-of-flight, structured-light and active stereoscopy technologies. Springer Nature, 2018.

[22] Ham, Hanry, Julian Wesley, and Hendra Hendra. "Computer vision based 3D reconstruction: A review." International Journal of Electrical and Computer Engineering 9.4 (2019): 2394.

[23] Mishra, D. K., and M. Chandwani. "CCD camera based automatic dimension measurement and reproduction of 3-D objects." Proceedings of TENCON'93. IEEE Region 10 International Conference on Computers, Communications and Automation. Vol. 4. IEEE, 1993 .

[24] Wang, J. G., and Y. F. Li. "3D object modeling using a binocular vision system." IMTC/99. Proceedings of the 16th IEEE Instrumentation and Measurement Technology Conference (Cat. No. 99CH36309). Vol. 2. IEEE, 1999.

[25] Gennery, Donald B. "Stereo-camera calibration." Proceedings ARPA IUS Workshop. Vol. 1. 1979.

[26] Jokela, Maria, Matti Kutila, and Long Le. "Road condition monitoring system based on a stereo camera." 2009 IEEE 5th International conference on intelligent computer communication and processing. IEEE, 2009.

[27] Liu, Yanqing, et al. "Real-time robust stereo visual SLAM system based on bionic eyes." IEEE Transactions on Medical Robotics and Bionics 2.3 (2020): 391-398.

[28] Zhang, Hongxin, and Suan Lee. "Robot bionic vision technologies: A review." Applied Sciences 12.16 (2022): 7970.

[29] Henseler, Helga, et al. "Investigation into accuracy and reproducibility of a 3D breast imaging system using multiple stereo cameras." Journal of Plastic, Reconstructive & Aesthetic Surgery 64.5 (2011): 577-582.

[30] Cadena, César, et al. "Robust place recognition with stereo cameras." 2010 IEEE/RSJ International Conference on Intelligent Robots and Systems. IEEE, 2010.

[31] Zhao, Peng, and Ni-Hong Wang. "Precise perimeter measurement for 3D object with a binocular stereo vision measurement system." Optik 121.10 (2010): 953-957.

[32] Yang, Shoubo, et al. "A calibration method for binocular stereo vision sensor with short-baseline based on 3D flexible control field." Optics and Lasers in Engineering 124 (2020): 105817.

[33] Sun, Lu, et al. "Non-contact optical sensing of asphalt mixture deformation using 3D stereo vision." Measurement 85 (2016): 100-117.

[34] Gennery, Donald B. "Stereo vision for the acquisition and tracking of moving three-dimensional objects." Machine Intelligence and Pattern Recognition. Vol. 3. North-Holland, 1986. 53-74.

[35] Aguilar, Juan-José, F. Torres, and M. A. Lope. "Stereo vision for 3D measurement: accuracy analysis, calibration and industrial applications." Measurement 18.4 (1996): 193-200.

[36] Liu, Yan, et al. "Wing deformation measurement using the stereo-vision methods in the presence of camera movements." Aerospace Science and Technology 119 (2021): 107161.

[37] Li, Jinjun, et al. "New 3D high-accuracy optical coordinates measuring technique based on an infrared target and binocular stereo vision." Optical Measurement Systems for Industrial Inspection VI. Vol. 7389. SPIE, 2009.

[38] O'Riordan, Andrew, et al. "Stereo vision sensing: Review of existing systems." 2018 12th International Conference on Sensing Technology (ICST). IEEE, 2018.

[39] Spampinato, Giacomo, et al. "Stereo vision based navigation for automated vehicles in industry." 2009 IEEE Conference on Emerging Technologies & Factory Automation. IEEE, 2009.

[40] Wang, Shaobo, et al. "Tracking a golf ball with high-speed stereo vision system." IEEE Transactions on Instrumentation and Measurement 68.8 (2018): 2742-2754.

[41] Lee, ChaBum, and Xiangyu Guo. "Spatially resolved stereoscopic surface profiling by using a feature-selective segmentation and merging technique." Surface Topography: Metrology and Properties 10.1 (2022): 014002.

[42] Guo, Xiangyu, and ChaBum Lee. "Fluorescence strobo-stereoscopy for specular reflection-suppressed full field of view imaging." Measurement 192 (2022): 110907.

[43] Guo, Xiangyu, and ChaBum Lee. "Preliminary study of phase-shifting strobo-stereoscopy for cutting tool monitoring." Journal of Manufacturing Processes 64 (2021): 1214-1222.

[44] Matsumoto, Yoshio, and Alexander Zelinsky. "An algorithm for real-time stereo vision implementation of head pose and gaze direction measurement." Proceedings Fourth IEEE International Conference on Automatic Face and Gesture Recognition (Cat. No. PR00580). IEEE, 2000.

[45] Yang, Sung-Pyo, et al. "Compact stereo endoscopic camera using microprism arrays." Optics letters 41.6 (2016): 1285-1288.

[46] Zhang, Zhengyou. "Microsoft kinect sensor and its effect." IEEE multimedia 19.2 (2012): 4-10.

[47] Logozzo, Silvia, et al. "Recent advances in dental optics–Part I: 3D intraoral scanners for restorative dentistry." Optics and Lasers in Engineering 54 (2014): 203-221.

[48] Shaukat, Affan, et al. "Towards camera-LIDAR fusion-based terrain modelling for planetary surfaces: Review and analysis." Sensors 16.11 (2016): 1952.

[49] Liu, Y., et al. "Foundations and Trends in Computer Graphics and Vision." Computational symmetry in computer vision and computer graphics 5.1-2 (2010): 1-195.

[50] Chandler, Jim, and Simon Buckley. "Structure from motion (SFM) photogrammetry vs terrestrial laser scanning." (2016).

[51] Goesele, Michael, Brian Curless, and Steven M. Seitz. "Multi-view stereo revisited." 2006 IEEE Computer Society Conference on Computer Vision and Pattern Recognition (CVPR'06). Vol. 2. IEEE, 2006.

[52] Goesele, Michael, et al. "Multi-view stereo for community photo collections." 2007 IEEE 11th International Conference on Computer Vision. IEEE, 2007.

[53] Wenzel, Konrad, et al. "Image acquisition and model selection for multi-view stereo." Int. Arch. Photogramm. Remote Sens. Spatial Inf. Sci 40.5W (2013): 251-258.

[54] Furukawa, Yasutaka, and Carlos Hernández. "Multi-view stereo: A tutorial." Foundations and Trends® in Computer Graphics and Vision 9.1-2 (2015): 1-148.

[55] Chiradejnant, Adit, Duangporn Suriyaamarit, and Mathawee Kaewprasert. "Calibration of an instrumented couch with a motioncapture system in measuring force applied and distance during manual therapy." Vajira Medical Journal: Journal of Urban Medicine 63.1 (2019): 1-8.

[56] Murmu, Narayan, Baisakhi Chakraborty, and Debashis Nandi. "Relative velocity measurement using low cost single camera-based stereo vision system." Measurement 141 (2019): 1-11.

[57] Kim, Hyongsuk, et al. "Distance measurement using a single camera with a rotating mirror." International Journal of Control, Automation, and Systems 3.4 (2005): 542-551.

[58] Zorgani, Ali, et al. "Optical elastography: tracking surface waves with digital image correlation." Physics in Medicine & Biology 64.5 (2019): 055007.

[59] Yang, Ning, Ju Huo, and Ming Yang. "A method for attitude measurement of a test vehicle based on the tracking of vectors." Measurement Science and Technology 26.8 (2015): 085019.

[60] Chen, Jixu, and Qiang Ji. "3D gaze estimation with a single camera without IR illumination." 2008 19th International Conference on Pattern Recognition. IEEE, 2008.

[61] Lloyd, Ryan, and Scott McCloskey. "Recognition of 3D package shapes for single camera metrology." IEEE Winter Conference on Applications of Computer Vision. IEEE, 2014.

[62] Lin, Huei-Yung, and Chun-Lung Tsai. "Depth measurement based on stereo vision with integrated camera rotation." IEEE Transactions on Instrumentation and Measurement 70 (2021): 1-10.

[63] Zhu, Jigui, Yanjun Li, and Shenghua Ye. "Design and calibration of a single-camera-based stereo vision sensor." Optical Engineering 45.8 (2006): 083001-083001.

[64] Sun, Y. Y. "A survey of 3D reconstruction based on single image." J North China Univ Technol 23.1 (2011): 9-13.

[65] Carpendale, M. Sheelagh T., David J. Cowperthwaite, and F. David Fracchia. "Extending distortion viewing from 2D to 3D." IEEE Computer Graphics and Applications 17.4 (1997): 42-51.

3. *A SINGLE CAMERA UNIT-BASED THREE-DIMENSIONALSURFACE IMAGING TECHNIQUE

3.1. Overview

Inspecting surface features is an essential step in manufacturing quality control that helps reduce the flow of defective products to the marketplace [1-3]. The industry has focused on contact 3D inspection techniques for decades, but traditional contact 3D inspection can no longer keep up with the pace of production. The industry is gradually moving to optical-based, non-contact 3D inspection [4,5].

This proposed single camera based stereoscopy built a precise motion system and used a CCD camera for image acquisition. The principles and techniques of the proposed inspection method are described, and the experimental setup is demonstrated. The 3D reconstruction from a single camera unit-based 3D surface imaging technique, compared with the conventional stereoscopic technique, obtains a better thickness calculation accuracy and surface feature extraction ability.

3.2. Preface

As industry and academia increasingly demand compact 3D surface imaging techniques, optics-based techniques are considered an affordable, highly efficient method to achieve 3D reconstruction [6,7]. The conventional stereoscopic measurement system has disadvantages such as a) constant baseline, b) low mobility, c) complex calibration, and d) high space consumption. In this research, a single-camera system-based stereoscopy was proposed to avoid such alignment,

* This research has been submitted to the International Journal of Precision Engineering and Manufacturing Journal and is under review.

calibration, and disparity error problems in conventional stereoscopy. Unlike conventional stereoscopy, which requires a pair of imaging devices, 3D surface imaging was achieved by 3D image reconstruction from two images taken from two different camera positions. The proposed imaging and calibration procedures are discussed below and compared with those of traditional stereoscopy.

3.3. Measurement method

Through the movement of the target or imaging devices, two images of the target at different locations are obtained by scanning. Then the 3D surface image can be reconstructed using the stereoscopy algorithm.

3.3.1. Stereoscopic imaging system

The conventional stereoscopic technique is implemented with a pair of imaging devices to acquire multi-view images of the target at different locations. The methodology schematic of the stereoscopy metrology is presented in Figure 3.1. The coordinate of an object point G in the global SRS (Spatial Reference System) are (X_G, Y_G, Z_G), and the point is projected onto the image plane of the left and right imaging devices, respectively. In the left imaging plane SRS, the coordinates of the projection point P_l are(X_{pl}, Y_{pl}) and the projection point P_r in the right imaging plane SRS are (X_{pr}, Y_{pr}).

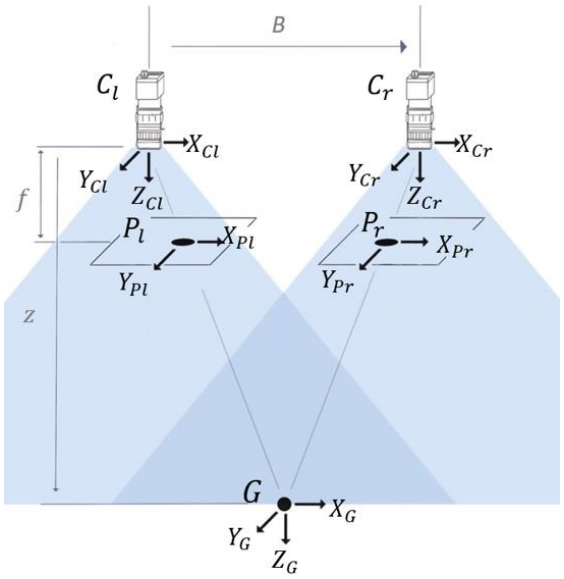

Figure 3.1. The principle of conventional stereoscopy.

In the schematic above, z represents the distance from the target to the imaging device, f represents the imaging device's effective focal length, and B is the baseline between a pair of imaging devices.

Based on the principle of projective geometry, the disparity between two images and the depth of the target can be calculated as [8]:

$$z = \frac{Bf}{x_{Pr} - x_{Pl}} \tag{3.1}$$

Where $x_{Pr} - x_{Pl}$ is the disparity between two images.

The global SRS of the detected object point G is calculated as follows [9-10]:

$$X_G = \frac{x_{Pl} z}{f} \tag{3.2}$$

$$Y_G = \frac{y_{Pl} z}{f} \tag{3.3}$$

3.3.2. Single camera unit-based 3D surface imaging technique

Based on the 3D image reconstruction principle described above, an image taken at a single position cannot generate disparity However, the disparity can be calculated by adjusting the relative position of the imaging device or the target, since the parameter obtained from two views is sufficient for triangulation and 3D image reconstruction. Using the geometric transformation described in Figure 3.2, a virtual imaging device can be made equivalent. The virtual imaging device at C_r shares the same corrected calibration matrix ($K_l = K_r$) as the physical imaging device C_l. The corrected calibration matrix (K) taking into account the non-square and non-perpendicular aspect of the pixels and the calibration matrix is shown below:

$$K = \begin{bmatrix} fm_x & s & c_x \\ 0 & fm_y & c_y \\ 0 & 0 & 1 \end{bmatrix} \tag{3.4}$$

Where skew parameter $s = fcos(\alpha)$ introduces this correction, α being the angle between two sides of the pixel. And m_x and m_y represent the number of pixels per length unit along the X- and Y-axes. The values of c_x and c_y correspond to the optical center coordinates in pixels at the lower left corner of the sensor.

This calibration process is relatively simple and fast compared to conventional stereoscopic techniques. This is because, in the conventional method, the intrinsic parameters of each imaging device ($K_l and\ K_r$) require independent calibration.

The stereoscopic technique can achieve accurate 3D reconstruction with high speed and superior stereo matching ability. Conventional stereoscopy requires two imaging devices with precisely calibrated internal and external parameters. In some industrial scenarios, the space is too limited to accommodate a pair of imaging devices, and the system alignment is greatly affected by environmental factors. In this theory, a novel 3D reconstruction method is proposed where only a single imaging device is used for stereo vision. Two experiments were designed to evaluate the proposed methods.

In method #1, the setup is shown in Figure. 3.2a. The imaging device is stationary, and the target motion is in a horizontal direction. Two images of the target were captured from different perspectives (C_L& C_R). On the other hand, in method #2 as depicted in Figure. 3.2b, the target is stationary, and the imaging device motion is in a horizontal direction. Two images of the target were captured from different perspectives (C_L& C_R).

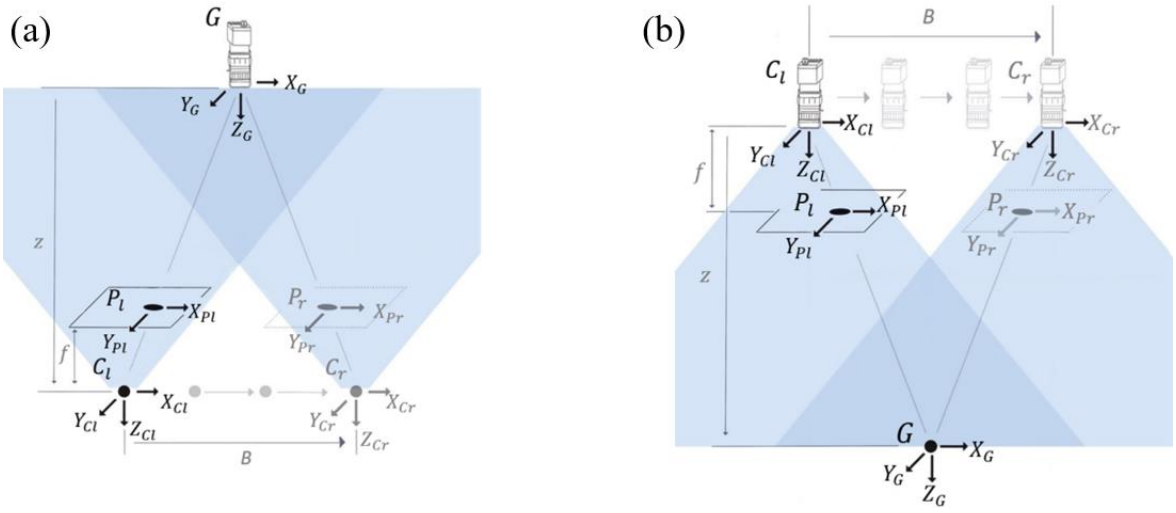

Figure 3.2. The proposed stereoscopy: (a) method #1 and (b) method #2.

3.4. Experiments

3.4.1. Experimental system

To evaluate the performance of the single camera unit-based 3D imaging technique, two independent vision systems were built under laboratory conditions. The configuration of method #1 is illustrated in Figure 3.3a. The camera was fixed to a table clamp attached to an optical breadboard, and the precision linear stage controlled by a stepper motor was used to move the target for scanning. On the other hand, in method #2, as shown in Figure 3.3b, the target was fixed on an optical stage and a UFACTORY xArm 6 Collaborative Robot was used to move the camera for scanning. The robotic system has a repeatability of ±0.1 mm.

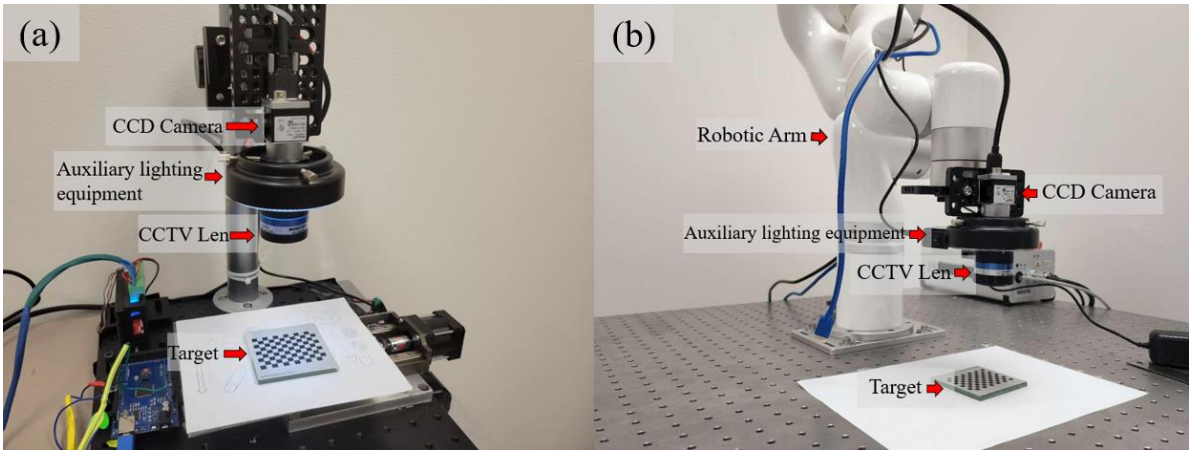

Figure 3.3. Experimental setup: (a) method #1 and (b) method #2.

For verification purposes, a CCD laser displacement sensor-based measurement system was constructed to measure the thickness of the specimen shown in Figure 3.4. A Keyence LK-G35 laser displacement sensor with 50 nm repeatability was mounted on an optical stage. The sample was placed on a Trilogy single-axis linear stage (0.1 μm accuracy). The line scan data of the target thickness was set as the reference value.

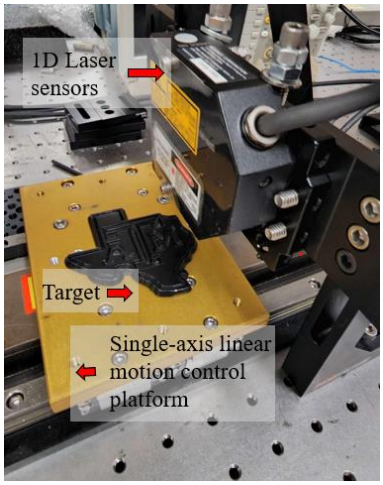

Figure 3.4. Displacement sensing system.

All experimental configurations use the same imaging device, the Basler acA5472-17 CCD camera, to acquire images. The camera is a CMOS with a sensor size of 13.1 mm × 13.1 mm and a resolution of 5472 pixels × 3648 pixels, and the pixel size of the imaging system is 2.4 μm × 2.4 μm. The camera is equipped with a Moritex ML-U1217SR-18C lens with a focal length of 12 mm. The imaging system includes an illumination device with a ring-shaped LED. Data were processed in the MATLAB and LABVIEW environments.

3.4.2. Calibration

Calibration is an essential step in determining the camera's internal and external parameters, the accuracy of which dramatically affects the quality of the 3D reconstruction [11-15]. An alumina calibration checkerboard with a square side length of 0.5 mm and an accuracy of ±20 um was used as the calibration target, as shown in Figure 3.5.

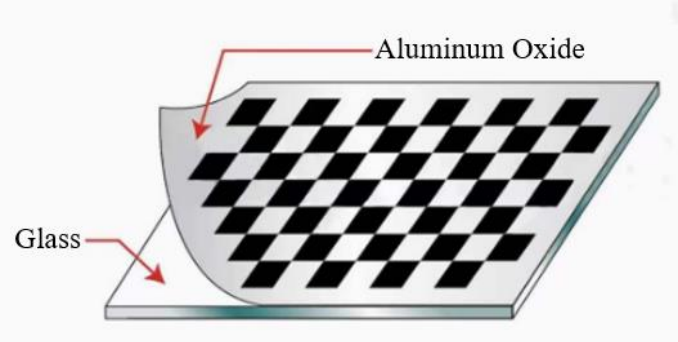

Figure 3.5. The material property of the GP070 calibration checkerboard.

Based on the principle in Section 2.3.3, two images of the calibration target can be captured by the camera during target or camera movement. 50 groups of checkerboard images were taken at different positions for system calibration, as shown in Figure 3.6. For a single camera system, camera #2 has the same parameters as camera #1 because it is an equivalent camera that does not physically exist. The camera calibration was performed using the Stereo Camera Calibrator application in MATLAB, which adopted Zhang's calibration algorithm [16-18].

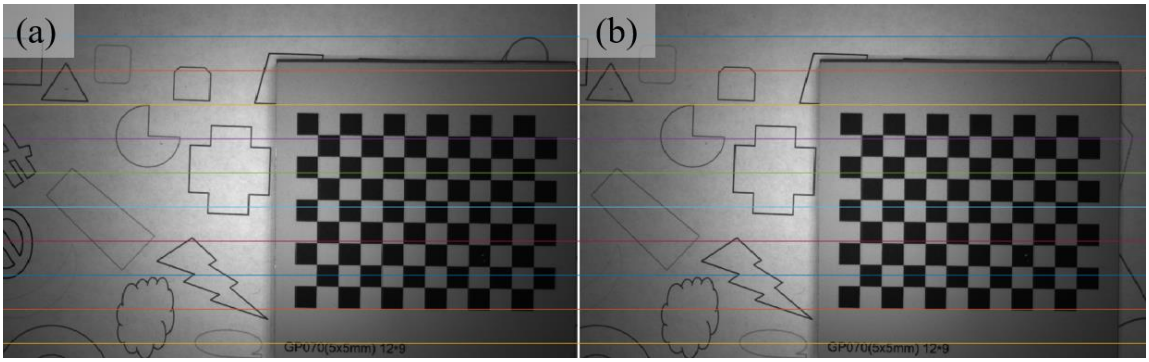

Figure 3.6. A pair of checkerboard images for camera calibration: (a) left location and (b) right location.

The histograms of the reprojection errors of method 1, method 2, and conventional are shown in Figure. 3.7, and the calibration results of the camera system are shown in Table 3.1.

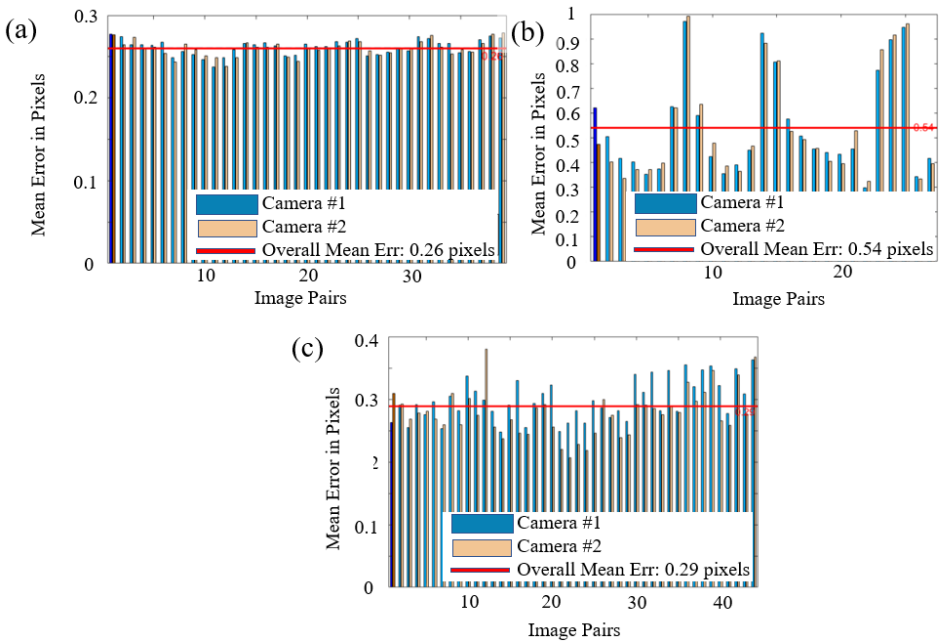

Figure 3.7. Reprojection error histogram: (a) method #1, (b) method #2, and (c) conventional method.

Table 3.1. Comparison of reprojection errors of two proposed methods and conventional methods.

	Method #1	Method #2	Conventional method
Reprojection Error (pixel)	0.26	0.54	0.29

3.4.3. Image acquisition

3.4.3.1. Experiment: Method #1

In the first experiment, the setup Arduino IDE sends the digital signal to the stepper motor controller to scan the sample target. The target is placed in the center of the camera's field of view. We installed a cross laser emitter behind the camera to adjust its orientation on the

target by specular projection. In a pair of images, the first image was taken when the stage moved -4.0 mm and the second image was taken when the stage moved in the opposite direction to +4.0 mm.

3.4.3.2. Experiment: Method #2

Instead of moving the target, the camera was moved in the Method #2 experiment. The camera was attached to the end effector of a robotic manipulator whose motion was controlled by a Python-coded program. As in method #1, a pair of images was taken, the first when the camera was moved to -4.0 mm and the second when the camera was moved to +4.0 mm. The camera's SRS can be calculated by matrix transformation of each motion position, and the system's external parameters can be obtained.

3.4.4. Thickness data processing

The result of 3D image reconstruction is directly affected by the quality of the raw image captured by the camera [19]. The reflections, shadows, electromagnetic interference, and other factors can cause noise in the 3D data, which affects the quality and accuracy of the thickness calculation. To improve the 3D reconstruction result, these unwanted noises must be suppressed by filter processing. The image processing is performed by the following steps: (1) Extract thickness data, (2) Separate the target and background, (3) Calculate the mean value of the background thickness, (4) Remove the mean value from both the target and background, (5) Filter the target and background separately, (6) Overlay the target and background to generate processed thickness data, (7) Reconstruct the 3D surface image. The process flowcharts are shown in Figure 3.8.

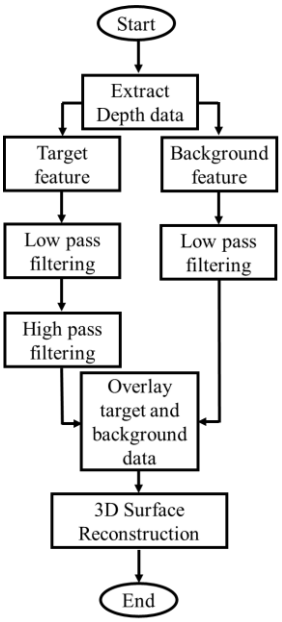

Figure 3.8. 3D image reconstruction process: flow chart.

To separate the target from the background, we use edge detection to find the boundaries of objects within the images. Considering the complexity of the background, we first convert the original image into a binary image based on the threshold to enhance the edge of the image to improve the contrast of the image. Then, morphology is applied to create structural elements according to the specified shape, and it is used to perform dilation, corrosion, and opening and closing operations on the structural elements of the target area [20,21]. The process of edge detection is illustrated in Figure. 3.9.

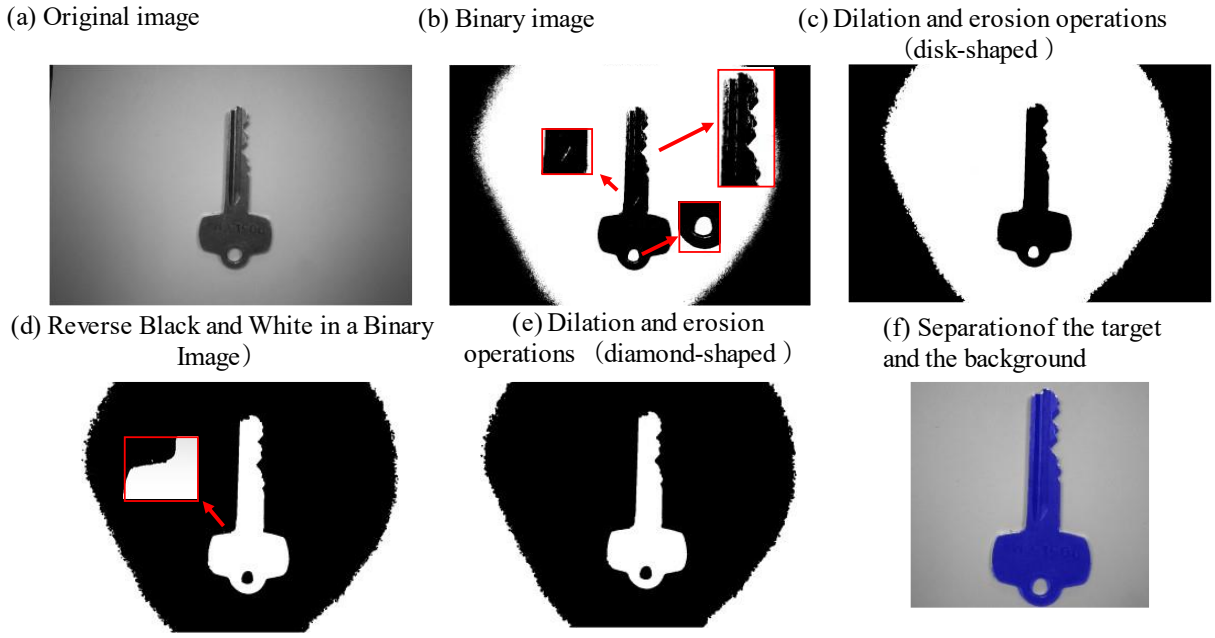

Figure 3.9. Edge detection process: results.

The pairing of pixels in the two images is critical to the disparity calculation. For objects that lack surface features or have a repeating texture, this mismatch can easily occur, resulting in a significant error in the disparity calculation example shown in Figure. 3.10 [22-24].

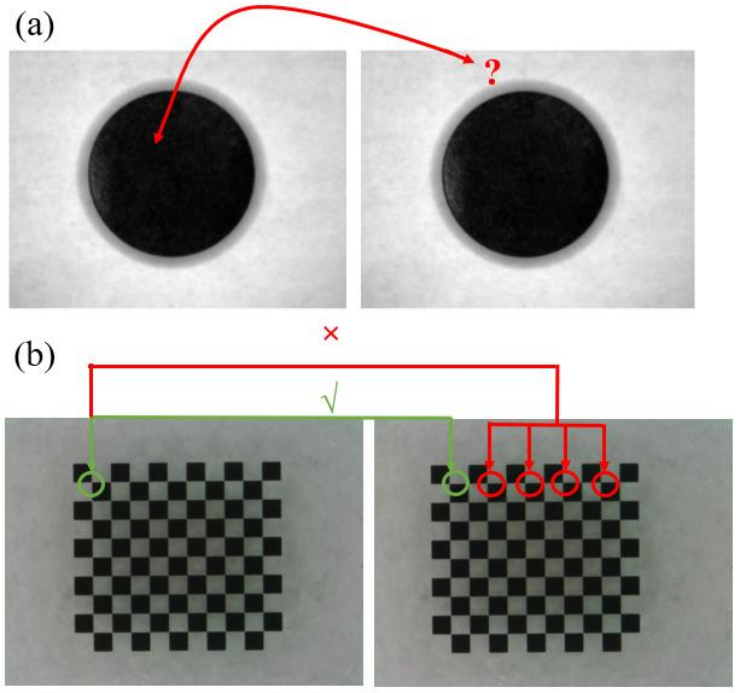

Figure 3.10. Examples of finding a match point: (a) missing texture, (b) repeating texture.

In this study, a unique background design was introduced to reduce the disparity error. The background is mainly white and filled with irregular geometric patterns (Figure 3.11). When the target has no surface features, the algorithm can pick up feature points in the background that can be used for matching. This unique texture design can reduce the feature point matching error in low-texture images, thereby reducing the disparity computation error (Figure 3.12b).

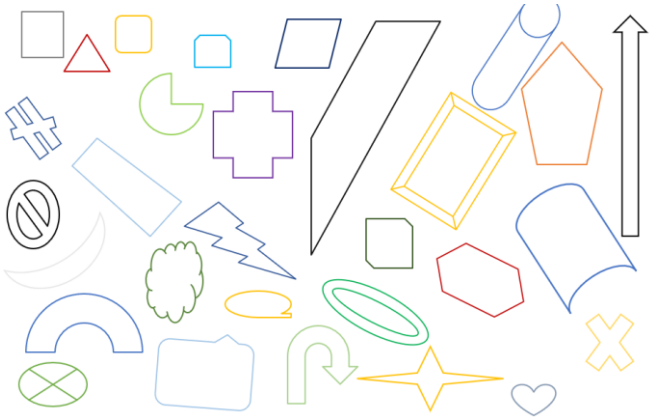

Figure 3.11. Background texture design.

The edge detection algorithm was used to separate the target from the background, the principle and experimental procedure can be referred to above. It is possible to have a deviation of a few pixels in edge detection, which may cause some background points to be classified as the target, or the target to appear as the background. This could cause a significant error in the depth calculation at the edge. To reduce the effect of the above problems on the uncertainty of the thickness measurement accuracy, after the target edge is detected, as shown in the red circle in Figure. 3.12c, the mask of the target is obtained by reducing 10 pixels from the edge. As shown by the green circle in Figure. 3.12d, the background mask is obtained by expanding 10 pixels from the edge, as shown by the blue circle in Figure. 3.12e.

To evaluate the performance of the thickness estimation, a linear measurement was performed horizontally along the center of the circle (Figure 3.12g). The comparison of raw and processed data is shown in Figure 3.12h.

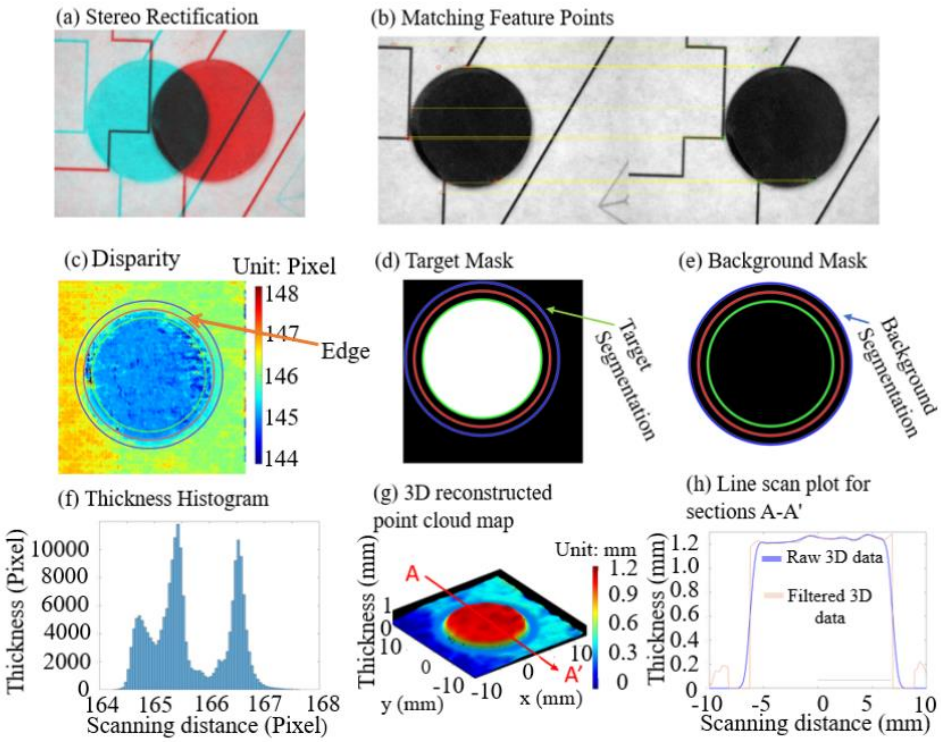

Figure 3.12. 3D image reconstruction process: results.

3.4.5. Regular geometry & simple surface features

The proposed single camera unit based 3D imaging technique measured the round geometry sample under laboratory conditions. The sample has a thickness of 1.20 mm and a radius of 7.50 mm (Figure. 3.13). The 3D point cloud map of the surface reconstruction along with the results of the central horizontal linear scan are shown in Figures 3.14 and 3.15. A similar pattern was observed at the center of the linear line. The ability to extract the surface feature on the target was validated by the experimental results.

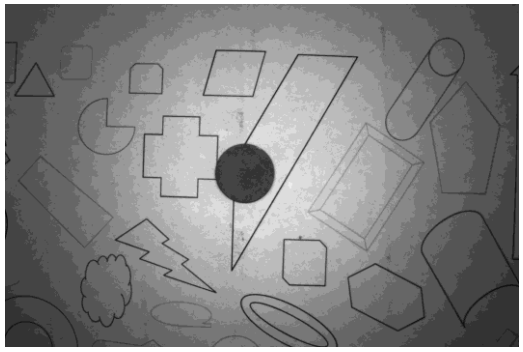

Figure 3.13. Camera view of the measured target.

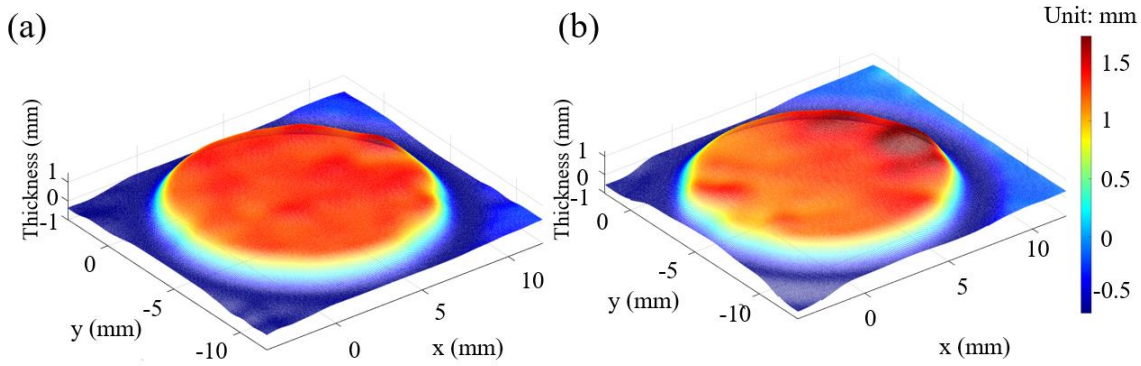

Figure 3.14. 3D image reconstruction point cloud results: (a) method #1 and (b) method #2.

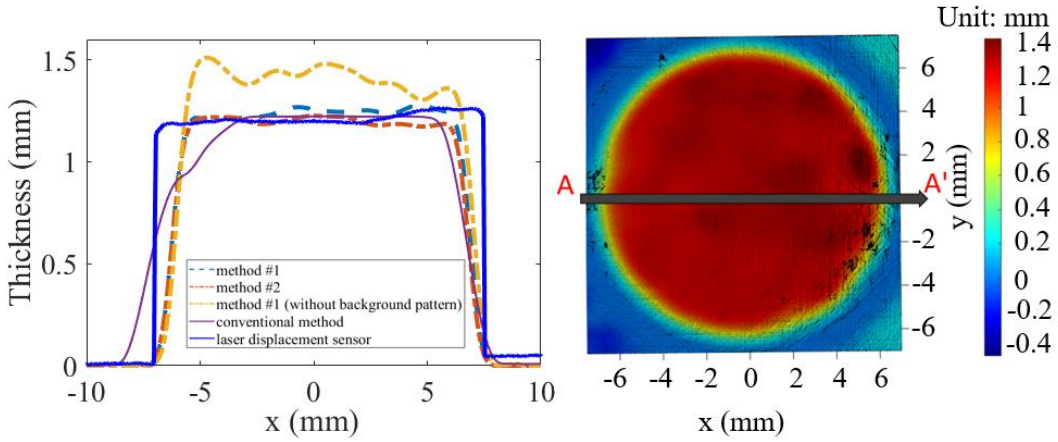

Figure 3.15. Experimental result: 3D image and its line profiles obtained by different methods.

The 3D point cloud map was drawn to validate the reconstruction performance. The mean value of the detected thickness obtained by different methods is shown in Table 3.2. Compared with the laser displacement sensor result, the measured thickness from both experiments was accurate with a relative error of less than 3%, as shown in Figure 3.15. The larger error in method #2 could be caused by the motion error of the robot arm, which can increase the multi-axis motion error during scanning. In addition, the feature profiles of method #1 were measured without the background pattern and using a conventional two-camera-based imaging system. The output of the laser displacement sensor was considered as the baseline data. The averaged thickness measured by method #1 and conventional stereoscopy showed 0.10 mm and 0.02 mm higher than the baseline data, respectively. From these experimental results, it was confirmed that method #1 with a single camera system, target scanning unit, and background pattern to reduce disparity error can be used for 3D surface imaging.

Table 3.2. Comparison of line scanning results: profile A-A' in Figure 3.15.

	Method #1	**Method #2**	**Method #1 (no background pattern)**	**Conventional method**	**Laser displacement sensor**
Averaged thickness	1.20 mm	1.24 mm	1.30 mm	1.22 mm	1.20 mm

3.4.6. Irregular geometry & complex surface features

The experimental results showed that the single camera unit-based 3D imaging technique can provide a complete surface reconstruction map. We increase the surface complexity, especially for the irregular ravines. A matte black metal Texas A&M University logo was selected to validate the performance of the surface feature extraction. The 3D reconstruction process follows the same principle as the cylindrical sample. The 3D point cloud map of the surface reconstruction results is shown in Figure 3.16.

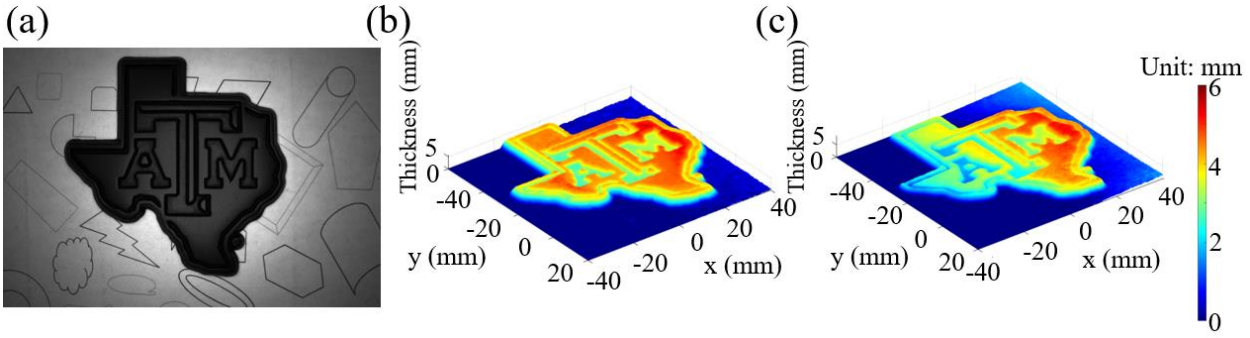

Figure 3.16. 3D reconstruction point cloud results: (a) camera view image of the test sample, (b) method #1, and (c) method #2.

Figure 3.16 shows that the 3D results obtained by method #1 could represent the shape of the sample, indicating that the proposed method can perform accurate measurements of samples with complicated geometries. However, in method #2, there may be misalignment and motion error of the robot arm, which may also cause tilt error, making the whole structure appear to be tilted.

3.5. References

[1] Li, Yadong, and Peihua Gu. "Free-form surface inspection techniques state of the art review." Computer-Aided Design 36.13 (2004): 1395-1417.

[2] Dowllng, M. M., et al. "Statistical issues in geometric feature inspection using coordinate measuring machines." Technometrics 39.1 (1997): 3-17.

[3] Li, Yadong, and Peihua Gu. "Inspection of free-form shaped parts." Robotics and Computer-Integrated Manufacturing 21.4-5 (2005): 421-430.

[4] Gao, J., N. Gindy, and X. Chen. "An automated GD&T inspection system based on non-contact 3D digitization." International journal of production research 44.1 (2006): 117-134.

[5] Baeg, Moon-Hong, et al. "A new robotic 3D inspection system of automotive screw hole." International Journal of Control, Automation, and Systems 6.5 (2008): 740-745.

[6] Mishra, D. K., and M. Chandwani. "CCD camera based automatic dimension measurement and reproduction of 3-D objects." Proceedings of TENCON'93. IEEE Region 10 International Conference on Computers, Communications and Automation. Vol. 4. IEEE, 1993.

[7] Wang, J. G., and Y. F. Li. "3D object modeling using a binocular vision system." IMTC/99. Proceedings of the 16th IEEE Instrumentation and Measurement Technology Conference (Cat. No. 99CH36309). Vol. 2. IEEE, 1999.

[8] Giancola, Silvio, Matteo Valenti, and Remo Sala. A survey on 3D cameras: Metrological comparison of time-of-flight, structured-light and active stereoscopy technologies. Springer Nature, 2018.

[9] Majumdar, Jharna. "Efficient parallel processing for depth calculation using stereo." Robotics and autonomous systems 20.1 (1997): 1-13.

[10] Zhao, Peng, and Ni-Hong Wang. "Precise perimeter measurement for 3D object with a binocular stereo vision measurement system." Optik 121.10 (2010): 953-957.

[11] Faugeras, Olivier, and Olivier Autor Faugeras. Three-dimensional computer vision: a geometric viewpoint. MIT press, 1993.

[12] Gennery, Donald B. "Stereo-camera calibration." Proceedings ARPA IUS Workshop. Vol. 1. 1979.

[13] Caron, Guillaume, and Damien Eynard. "Multiple camera types simultaneous stereo calibration." 2011 IEEE International Conference on Robotics and Automation. IEEE, 2011.

[14] Rathnayaka, Pathum, Seung-Hae Baek, and Soon-Yong Park. "An efficient calibration method for a stereo camera system with heterogeneous lenses using an embedded checkerboard pattern." Journal of sensors 2017 (2017).

[15] Wang, Jian, et al. "High-Accuracy Calibration of High-Speed Fringe Projection Profilometry Using a Checkerboard." IEEE/ASME Transactions on Mechatronics 27.5 (2022): 4199-4204.

[16] Zhang, Zhengyou. "A flexible new technique for camera calibration." IEEE Transactions on pattern analysis and machine intelligence 22.11 (2000): 1330-1334.

[17] Li, Wei, et al. "A practical comparison between zhang's and tsai's calibration approaches." Proceedings of the 29th International Conference on Image and Vision Computing New Zealand. 2014.

[18] Burger, Wilhelm. "Zhang's camera calibration algorithm: in-depth tutorial and implementation." HGB16-05 (2016): 1-6.

[19] Gartner, William C. "Image formation process." Journal of travel & tourism marketing 2.2-3 (1994): 191-216.

[20] Maragos, Petros. "Tutorial on advances in morphological image processing and analysis." Optical engineering 26.7 (1987): 623-632.

[21] Serra, Jean, and Pierre Soille, eds. Mathematical morphology and its applications to image processing. Vol. 2. Springer Science & Business Media, 2012.

[22] Scharstein, Daniel, and Richard Szeliski. "A taxonomy and evaluation of dense two-frame stereo correspondence algorithms." International journal of computer vision 47 (2002): 7-42.

[23] Mühlmann, Karsten, et al. "Calculating dense disparity maps from color stereo images, an efficient implementation." International Journal of Computer Vision 47 (2002): 79-88.

[24] Qin, Shaodong, and Mladen Berekovic. "A comparison of high-level design tools for soc-fpga on disparity map calculation example." arXiv preprint arXiv:1509.00036 (2015).

4. ERROR ANALYSIS

In the following, we will introduce physical and mathematical methods to mitigate the effects of motion error on 3D reconstruction accuracy.

4.1. Tilt Error

For a stereoscopic imaging system, the angle of the target and the camera should ideally be identical during calibration and measurement. Subtle angular transformations between the target and the camera can cause errors in the disparity calculation, resulting in failure of the 3D reconstruction. In traditional cases, we are forced to adjust the position of the camera and recalibrate the camera system. Take advantage of the multi-axis freedom of the robot manipulator. We can change the robot's pose so that the camera and the target can regain the angle of the original calibration.

The "Roosevelt" design of the United States 10-cent coin was chosen as a test sample. First, the sample was mounted on a goniometer stage at an angle of 25 degrees and the stereo image was captured in its original position. Second, a robot was used to tilt the camera by 25 degrees so that the camera and target were in a vertical position.

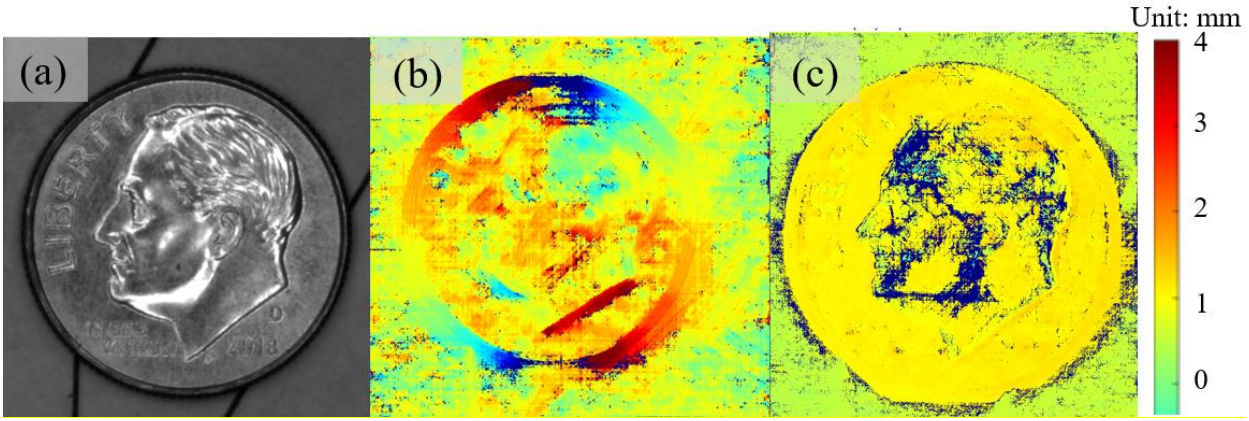

Figure 4.1. 3D image reconstruction results: (a) original image and (b) disparity maps without robot aid and (c) disparity maps with robot aid.

Comparing the two disparity maps in Figure 4.1, we can clearly see that when the calibration and measurement angles change, the quality of the disparity map decreases. However, if we use the robot to compensate for its tilt error, we can obtain an accurate disparity map. Using a robot, the camera system was able to measure a thickness of about 1.30 mm. compared to the coin specifications of 1.35 mm. The thickness discrepancy was only 3.70% and the disparity map clearly shows the head of President Roosevelt on the coin. For reference, the blue areas in Figure 4.1c are caused by the highly reflective areas where the thickness calculation result may have a large error with the true value, whose thickness is assigned as an unrepresentable value or known as Not a Number (NaN) by filter processing to ensure the accuracy of the overall thickness calculation.

4.2. Baseline Error

Ideally, the baseline distance should be consistent when performing camera calibration. (B_c) and actual measurement (B_m). When $B_c = B_m$. We can define the measured thickness as the true

value.(Z_t), assuming no measurement error and no calculation error during the measurement process. In many cases, camera setup and baseline in complex industrial environments are affected by many uncontrollable factors that may not be able to be calibrated to the ideal baseline length. Also, the Pose Repeatability (RP) and Pose Accuracy (AP) of the robot manipulator are affected by both kinematic error and non-kinematic error, etc [1-2]. Therefore, in actual applications cases, the measured thickness (Z_m) and the true thickness (Z_t) are not identical due to the baseline error.

According to equation 3.1 and the measurement method above. The disparity has a proportional relationship with the baseline distance based on triangulation.

$$\frac{B_c}{d_c} = \frac{B_m}{d_m} \tag{4.1}$$

Where d_c is the disparity between two images during camera calibration and d_m is the disparity between two images during the actual measurement.

The measured thickness equation can be rewritten based on the above relationship as follows:

$$Z_m = \frac{B_c f}{d_m} = \frac{B_c f}{\frac{B_m}{B_c} d_c} = \frac{B_c}{B_m} Z_t = \beta\, Z_t \tag{4.2}$$

The above equation indicates that there is a positive relationship between Z_m and β. To verify this theory, the target with a thickness of 1.65 mm and a radius of 7.50 mm was selected as the reference for this experiment. The camera system was calibrated with a baseline of 8.0 mm. Ten groups of stereo images were collected at a constant rate of change of 0.625 mm in baseline distance.

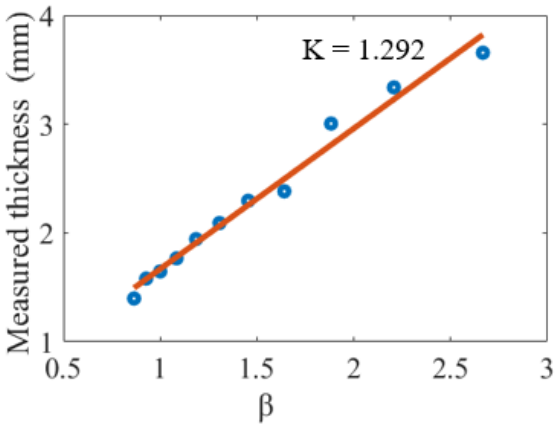

Figure 4.2. Experimental result: curve chart of measured thickness versus β.

The above graph (Figure 4.2) shows that the relationship between β and the measured thickness variation (Z_m.) is controllable and we can obtain the ratio of the regression sum of squares (SSR) and the total sum of squares (SST) equal to 0.9814. This experiment verifies the linear relationship between β and Z_m. The experiment shows that when using a single camera system, even if the calibration baseline length and the measurement baseline length are different, the true thickness of the measured target can still be recovered using Equation 4.2.

4.3. Summary

The single camera-based stereoscopy was developed and preliminarily validated with the sample test. Successful 3D surface imaging was achieved by 3D image reconstruction from a pair of images obtained either from two different camera positions or from two different target positions. In the proposed approach, two images could be obtained either by scanning the target object or by moving the camera system. The proposed method was effective in reducing the disparity error, avoiding the camera parameter discrepancy of the two imaging systems, and simplifying the camera calibration procedure. As a result, the proposed method improved the imaging result compared to conventional stereoscopy, which is limited to the disparity error in

3D image reconstruction because a pair of imaging devices is not ideally identical and there is always an alignment error in the imaging system setup.

4.4. References

[1] Chen, Jigien, and Lih-Ming Chao. "Positioning error analysis for robot manipulators with all rotary joints." IEEE Journal on Robotics and Automation 3.6 (1987): 539-545.

[2] Mavroidis, Constantinos, et al. "A systematic error analysis of robotic manipulators: application to a high performance medical robot." Proceedings of International Conference on Robotics and Automation. Vol. 2. IEEE, 1997.

5. CONCLUSIONS

5.1. Conclusion

The research work presented in this thesis includes the development and investigation of the novel single camera-based stereoscopy to address the current challenges and limitations of conventional stereoscopy, such as calibration error, space occupancy, and mobility, as a result, single camera-based stereoscopy can save up to 50% space occupancy and cost by reducing one imaging device. And it can be easily integrated with assembly line conveyor belts by using method #1 or comment with a robotic manipulator as method #2 for industrial production, this research has great potential to be commercialized. In addition, single camera-based stereoscopy has greater mobility, it has at least one degree of freedom. This allows the user to adjust the camera baseline to the size of the object without recalibration. Finally, single-camera stereoscopy can provide sub-millimeter errors in thickness measurement, which can be used for precision applications such as cutting tool monitoring. Therefore, single-camera-based stereoscopy has the potential to provide high-precision, non-contact measurement with advantages such as simplicity, cost-effectiveness, and efficiency.

5.2. Future Works

For future work, a stroboscopic instrument could be added to the current setup [1-4]. The proposed methods can also be applied to the measurement, characterization, and monitoring of various dynamic scenarios in dimensional metrology, as schematically shown in Figure 5.1. The 3D reconstruction at the microscale could also be achieved by using an objective lens instead of an ordinary zoom lens, and the new system could be used in high-precision 3D microscopy. This project is currently in its initial stages as a continuation of this theory. The schematic diagram and experimental setup are shown in Figure 5.2.

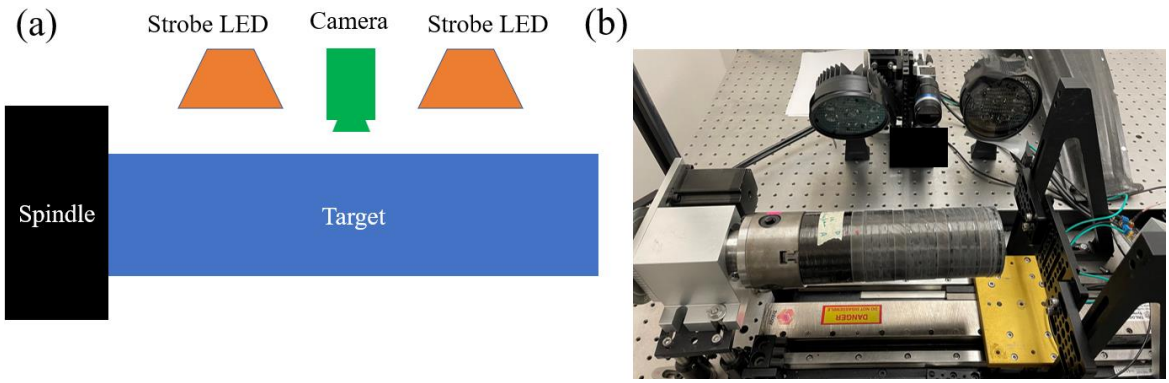

Figure 5.1. Single camera-based strobo stereoscopy: (a) schematic diagram and (b) Experimental setup.

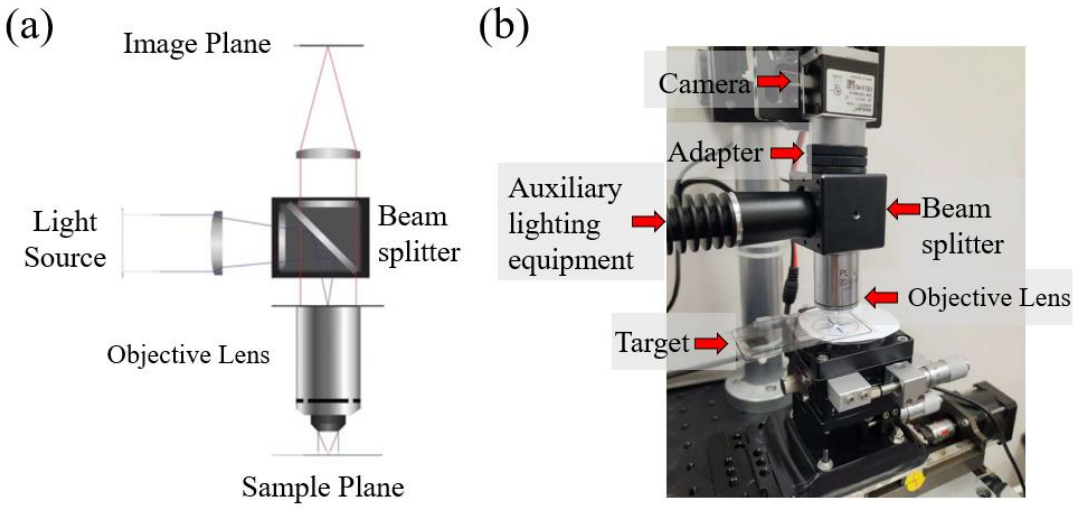

Figure 5.2. Single camera-based 3D microscopy: (a) schematic diagram and (b) experimental setup.

5.3. References

[1] Lee, ChaBum, and Xiangyu Guo. "Spatially resolved stereoscopic surface profiling by using a feature-selective segmentation and merging technique." Surface Topography: Metrology and Properties 10.1 (2022): 014002.

[2] Guo, Xiangyu, and ChaBum Lee. "Fluorescence strobo-stereoscopy for specular reflection-suppressed full field of view imaging." Measurement 192 (2022): 110907.

[3] Guo, Xiangyu, and ChaBum Lee. "Preliminary study of phase-shifting strobo-stereoscopy for cutting tool monitoring." Journal of Manufacturing Processes 64 (2021): 1214-1222.

[4] Wang, Shaobo, et al. "Tracking a golf ball with high-speed stereo vision system." IEEE Transactions on Instrumentation and Measurement 68.8 (2018): 2742-2754.